Cobalt Alters the Growth of a Manganese Oxide Film

Young-Shin Jun and Scot T. Martin*

Division of Engineering and Applied Sciences, 29 Oxford Street, Pierce Hall, Harvard University, Cambridge, Massachusetts 02138

Received April 10, 2005. In Final Form: September 1, 2005

The mobility of dissolved heavy metals in natural waters is partially regulated by interactions with manganese oxide films. In the current work, the effects of aqueous cobalt(II) on manganese oxide film growth are studied by atomic force microscopy. The film is grown on the $(10\bar{1}4)$ surface of rhodochrosite ($MnCO_3$). In the presence of O_2(aq) and at circumneutral pH, film growth begins as manganese oxide islands that expand laterally across the surface. Addition of Co^{2+}(aq) leads to the partial or complete dissolution of the manganese oxide film. Simultaneously, there is growth of new islands having multilayer structures that are unrestrained in the *z*-direction. The chemical composition of these new islands appears to include both Co and Mn ions. Empirical rules governing the growth of the two types of islands can be developed for the absence and the presence of Co^{2+}(aq). In the absence of Co^{2+}(aq), islands grow as flat two-dimensional rhombohedral islands of nearly uniform height (2.4 ± 0.3 nm). These islands do not cross over steps on the substrate. The growth rules change markedly in the presence of Co^{2+}(aq). The islands grow indefinitely in the *z*-direction as strata structures of polydisperse thickness and rounded tops. The islands readily grow over steps. Cobalt ions, therefore, relieve the two-dimensional restriction on layer formation and allow three-dimensional growth. Moreover, the shape of the dissolution pits on the surface of $MnCO_3$ changes from rhombohedral in the absence of cobalt to partially rounded in the presence of cobalt. The rounding occurs for the obtuse edges of the pit. Direct microscopic observations of the interactions of cobalt with manganese oxide films provide new mechanistic insights that are important in the quantitative modeling of the mobility of heavy metals in the environment.

1. Introduction

The mobility of dissolved heavy metals in aquatic environments is often affected by existing and newly formed oxide coatings (i.e., films).[1−4] Particularly widespread in soils and sediments are coatings of manganese oxides. Oxide coatings provide a surface for metal adsorption[5−8] and a medium for metal absorption.[5,9−11] Moreover, when the coatings dissolve, the associated metal ions are released.[12,13] A dynamic description of the fate and the transport of metal contaminants thus includes the thermodynamics and the kinetics of dissolution, precipitation, adsorption, and incorporation. Important regulators of these processes are pH, dissolved oxygen, and foreign ions such as heavy metal ions. At the macroscopic level, the interactions of heavy metal ions with manganese oxides have been studied extensively.[14−20] There is also significant, though less comprehensive, work at the microscopic level.[21−23]

One heavy metal of particular importance is cobalt. Cobalt is an essential micronutrient for phytoplankton growth in the oceans[24] and plays a critical role in the biomethylation of other heavy metals such as mercury.[25,26] Although only a few nanomolar aqueous cobalt is usually present in freshwaters, there is, nevertheless, significant environmental interest because ^{60}Co is radioactive and is a priority contaminant at defense-related sites.[25,27] Moreover, cobalt occurs in significant quantities in naturally occurring manganese oxides deposited from fresh and marine waters.[20]

Cobalt adsorption and oxidation have been previously studied on manganese oxides,[17,20,23,28,29] silicates,[30] rutile,[30] and clays.[13] Manceau et al.[23] found that Co^{2+} was oxidized exclusively by Mn^{III} rather than Mn^{IV} in the hydrogen-rich birnessite structure. O'Day et al.[30] studied the adsorption of Co^{2+}(aq) on quartz and rutile with X-ray absorption spectroscopy. On the rutile surface,

* To whom correspondence should be addressed. E-mail: scot_martin@harvard.edu.

(1) Stumm, W.; Morgan, J. J. *Aquatic Chemistry*; Wiley: New York, 1996.
(2) Villinski, J.; O'Day, P.; Corley, T.; Conklin, M. *Environ. Sci. Technol.* **2001**, *35*, 1157−1163.
(3) Fan, M.; Boonfueng, T.; Xu, Y.; Axe, L.; Tyson, T. A. *J. Colloid Interface Sci.* **2005**, *281*, 39−48.
(4) Papini, M. P.; Bianchi, A.; Grimaldi, C.; Behra, P. *Water, Air, Soil Pollut.* **2004**, *159*, 49−65.
(5) Muller, B.; Granina, L.; Ulrich, A.; Wehrli, B. *Environ. Sci. Technol.* **2002**, *36*, 411−420.
(6) Al-Abadleh, H. A.; Grassian, V. H. *Surf. Sci. Rep.* **2003**, *52*, 63−161.
(7) Brule, D. G.; Brown, J. R.; Bancroft, G. M.; Fyfe, W. S. *Chem. Geol.* **1980**, *28*, 331−339.
(8) Fuller, C. C.; Harvey, J. W. *Environ. Sci. Technol.* **2000**, *34*, 1150−1155.
(9) Towle, S. N.; Bargar, J. R.; Brown, G. E.; Parks, G. A. *J. Colloid Interface Sci.* **1997**, *187*, 62−82.
(10) Tournassat, C.; Charlet, L.; Bosbach, D.; Manceau, A. *Environ. Sci. Technol.* **2002**, *36*, 493−500.
(11) Duff, M. C.; Coughlin, J. U.; Hunter, D. B. *Geochim. Cosmochim. Acta* **2002**, *66*, 3533−3547.
(12) Brown, G. E.; Foster, A. L.; Ostergren, J. D. *Proc. Natl. Acad. Sci. U.S.A.* **1999**, *96*, 3388−3395.
(13) Thompson, H. A.; Parks, G. A.; Brown, G. E. *Geochim. Cosmochim. Acta* **1999**, *63*, 1767−1779.
(14) Hem, J. D. *Geol. Soc. Am. Bull.* **1972**, *83*, 443−450.
(15) Hem, J. D. *Chem. Geol.* **1978**, *21*, 199−218.
(16) Hem, J. D. *Geochim. Cosmochim. Acta* **1981**, *45*, 1369−1374.
(17) Hem, J. D.; Lind, C. J. *Geochim. Cosmochim. Acta* **1991**, *55*, 2435−2451.
(18) Hem, J. D.; Lind, C. J.; Roberson, C. E. *Geochim. Cosmochim. Acta* **1989**, *53*, 2811−2822.
(19) Hem, J. D. In *Particulates in Water*; Kavanaugh, M. C., Leckie, J. O., Eds.; American Chemical Society: Washington, DC, 1980; Vol. 189, pp 45−72.
(20) Hem, J. D.; Roberson, C. E.; Lind, C. J. *Geochim. Cosmochim. Acta* **1985**, *49*, 801−810.
(21) Fendorf, S.; Jardine, P. M.; Patterson, R. R.; Taylor, D. L.; Brooks, S. C. *Geochim. Cosmochim. Acta* **1999**, *63*, 3049−3057.
(22) Foster, A. L.; Brown, G. E.; Parks, G. A. *Geochim. Cosmochim. Acta* **2003**, *67*, 1937−1953.
(23) Manceau, A.; Drits, V. A.; Silvester, E.; Bartoli, C.; Lanson, B. *Am. Mineral.* **1997**, *82*, 1150−1175.
(24) Moffett, J. W.; Ho, J. *Geochim. Cosmochim. Acta* **1996**, *60*, 3415−3424.
(25) Lienemann, C.-P.; Taillefert, M.; Perret, D.; Gaillard, J.-F. *Geochim. Cosmochim. Acta* **1997**, *61*, 1437−1446.
(26) Harris, H. H.; Pickering, I. J.; George, G. N. *Science* **2003**, *301*, 1203.
(27) Xu, N.; Hochella, M. F.; Brown, G. E.; Parks, G. A. *Geochim. Cosmochim. Acta* **1996**, *60*, 2801−2815.
(28) Murray, J. W. *Geochim. Cosmochim. Acta* **1975**, *39*, 505−519.
(29) Murray, J. W. *Geochim. Cosmochim. Acta* **1975**, *39*, 635−647.
(30) O'Day, P. A.; ChisholmBrause, C. J.; Towle, S. N.; Parks, G. A.; Brown, G. E. *Geochim. Cosmochim. Acta* **1996**, *60*, 2515−2532.

10.1021/la0509450 CCC: $33.50
Published on Web 01/25/2006

cobalt substituted into octahedral coordination sites to replace Ti^{IV}. This result was explained by the similarity in the ionic radii (viz., 0.72 Å for Co^{II} and 0.68 Å for Ti^{IV}). In comparison, cobalt precipitated on the surface of quartz (0.41 Å for Si^{IV}) as cobalt hydroxide ($Co(OH)_2(s)$). Thompson et al.[13] employed extended X-ray absorption fine structure (EXAFS) spectroscopy to investigate the interfacial chemistry of dissolution, surface adsorption, and precipitation during the aging of a cobalt(II)−clay−water system. Lee and Tebo[31] reported that certain bacteria that oxidized Mn^{II} as an energy source could alternatively employ Co^{II} as a substrate: the standard reduction potentials of Co(II)/Co(III) as $Co^{III}OOH$ to Co^{2+}(aq) and Mn(II)/Mn(III) as $Mn^{III}OOH$ to Mn^{2+}(aq) are 1.48 and 1.50 V,[24] respectively, and Co and Mn ions can, therefore, sometimes play interchangeable roles in redox reactions in the environment. Taillefert et al.[32] demonstrated that the dynamic evolution of manganese oxide directly influenced the distribution of Co in the oxic−anoxic transition of a lacustrine water column. Aqueous cobalt was released during the reductive dissolution of manganese oxides and accumulated at the redox interface.

The results reported in the present paper focus on the effects of aqueous cobalt(II) ion on manganese oxide film growth on a rhodochrosite ($MnCO_3$) substrate. We previously reported that a manganese oxide film, in the absence of heavy metals, grows on the surface of rhodochrosite in the presence of O_2(aq) for $5.8 < pH < 7.7$.[33] The film results from the chemical oxidation by O_2(aq) of Mn^{2+}(aq) released from the dissolution of $Mn^{II}CO_3$ to form an oxide overgrowth. The surface morphology, aqueous manganese concentration, and substrate crystallography affect the orientation, the height, and the shape of the manganese oxide islands.[34] These islands grow laterally to form a contiguous film. The current study extends these earlier findings by investigating the effects of aqueous Co^{2+} on film growth.

2. Experimental Section

2.1. Sample Preparation. $MnCO_3$ (rhodochrosite, sample no. 96030, Colorado) was obtained from the Harvard University Mineralogical Museum and prepared as previously reported.[34,35] Impurities included 0.20% Zn and 0.17% Ca. Fresh, flat $(10\bar{1}4)$ surfaces were prepared by breaking a large (1 cm^3) crystal specimen with a razor blade. The average sample surface area was 5.3 mm^2. Without further treatment, samples were fixed on a steel disk with warm wax in preparation for imaging.

2.2. Atomic Force Microscopy. The surface was imaged using an atomic force microscope equipped with a fluid cell (Nanoscope IIIa Multimode SPM, Digital Instruments).[34,36,37] Contact-mode images were recorded every 4.3 min. The time series of images recorded film growth.

2.3. Protocols for Film Growth. In a typical experiment, a $MnCO_3$ surface was reacted with solutions introduced into the fluid cell of the atomic force microscope at a flow rate of 0.1 mL min^{-1}. Solutions were previously saturated with 1 atm of O_2 at 298 K by purging with oxygen gas for at least 2 h, the ionic strength was adjusted to 10^{-2} M with $NaNO_3$ (100%, Mallinckrodt), and the pH was set to 6.4 ± 0.1. Control experiments were also conducted in the absence of dissolved oxygen. Cobalt-containing solutions were prepared from $Co(NO_3)_2 \cdot 6H_2O$ (100%, Sigma); Co^{2+}(aq) speciated

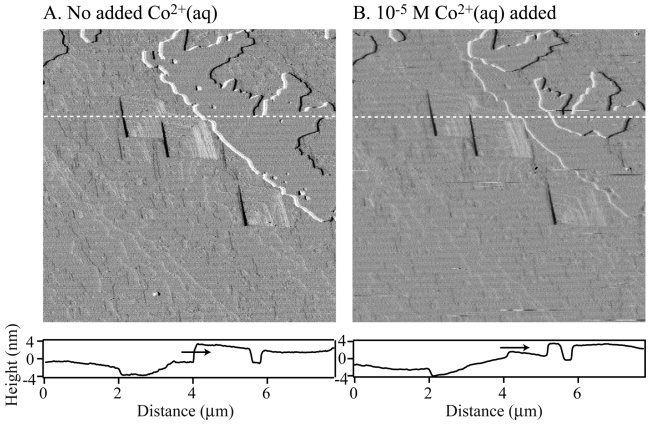

Figure 1. The manganese oxide film dissolves after cobalt is added. Micrograph A is obtained 1390 min after introduction of the cobalt-free aqueous solution. Micrograph B is obtained 230 min after introduction of 10^{-5} M Co^{2+}. Deflection-mode micrographs are 7.7 × 7.7 μm^2 for solution conditions of 298 K, pH 6.3, and 1 atm of O_2(aq). These solution conditions also hold for Figures 2−7.

98.4% as $Co(H_2O)_6^{2+}$ at pH 6.4. Effluent from the fluid cell was analyzed off-line for aqueous manganese and cobalt concentrations using a GF-AAS instrument (Perkin-Elmer AAnalyst 300).

Three complementary experimental protocols were employed to investigate the effects of Co^{2+}(aq) on film growth: (1) no Co^{2+}(aq) was added; (2) no Co^{2+}(aq) was added during the initial stages of film growth, but 10^{-3} to 10^{-6} M Co^{2+} was added in the later stages of film growth; and (3) 10^{-5} M Co^{2+} was added prior to and throughout all stages of film growth.

2.4. Thermodynamic Calculations. The measured aqueous concentrations of Mn^{2+} and Co^{2+} in the effluent of the fluid cell were employed to calculate the saturation ratios of solid manganese and cobalt phases (including oxides, hydroxides, and carbonates) to determine which were thermodynamically possible under our experimental conditions. Calculations were completed with MINEQL+ software (Environmental Research Software, Hallowell, ME).[38]

3. Results and Discussion

Our earlier work[34] establishes that the basic processes of manganese oxide film growth on $MnCO_3$ are as follows. Aqueous Mn^{2+} released during the dissolution of $MnCO_3$ adsorbs onto the $MnCO_3$ surface at circumneutral pH and, in the presence of 1 atm of dissolved oxygen, nucleates rhombohedral manganese(II/III) oxide islands to initiate film growth. The islands grow laterally and coalesce, and a thin manganese oxide film fully covers the substrate surface after sufficiently long exposure (12 h). In our usage, a film describes any overgrowth on a substrate. The growth can range from two-dimensional islands, which we call a patchy film, to a contiguous sheet, which we call a continuous film.

Our present work (Figure 1 and circled areas in Figure 2) shows that the manganese oxide film dissolves following the addition of cobalt ions (i.e., protocol 2). New islands simultaneously nucleate and grow (Figures 2 and 3). These observations indicate that the original manganese oxide film is of higher solubility than the new islands formed in the presence of cobalt ions, which therefore implies that the new islands are of a distinct chemical composition.

Dissolution of the manganese oxide layer simultaneous with new film growth may be explained by a thermodynamic ripening mechanism of the transformation from a solid of higher K_{sp} (i.e., the manganese oxide film) to a solid of lower K_{sp} (i.e., the new film). The rate of this process, in addition to water- or proton-

(31) Lee, Y.; Tebo, B. M. *Appl. Environ. Microbiol.* **1994**, *60*, 2949−2957.
(32) Taillefert, M.; MacGregor, B. J.; Gaillard, J. F.; Lienemann, C. P.; Perret, D.; Stahl, D. A. *Environ. Sci. Technol.* **2002**, *36*, 468−476.
(33) Duckworth, O. W.; Martin, S. T. *Geochim. Cosmochim. Acta* **2004**, *68*, 607−621.
(34) Jun, Y. S.; Kendall, T. A.; Martin, S. T.; Friend, C. M.; Vlassak, J. J. *Environ. Sci. Technol.* **2005**, *39*, 1239−1249.
(35) Duckworth, O. W.; Martin, S. T. *Am. Mineral.* **2004**, *89*, 554−563.
(36) Jun, Y. S.; Martin, S. T. *Environ. Sci. Technol.* **2003**, *37*, 2363−2370.
(37) Duckworth, O. W.; Martin, S. T. *Geochim. Cosmochim. Acta* **2003**, *67*, 1787−1801.
(38) Schecher, W. D.; McAvoy, D. C. *MINEQL+: A Chemical Equilibrium Modeling System*; Environmental Research Software: Hallowell, ME, 1998.

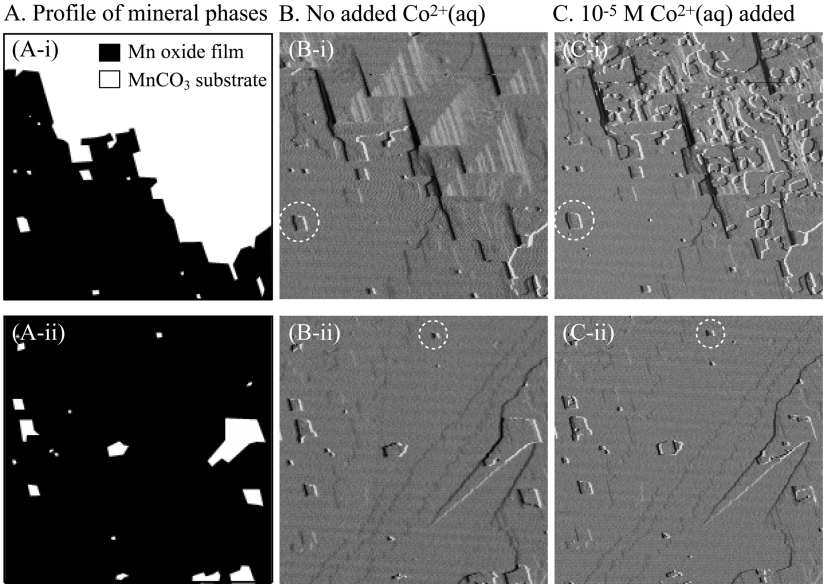

Figure 2. In the presence of cobalt, islands form at the bottom of the pits. The artwork in A, prepared in Adobe Photoshop, shows regions of $MnCO_3$ and manganese oxide film. Micrographs in B are obtained 1140 min after introduction of the aqueous solution. The manganese oxide film grows in the lower left-hand quadrant. Clean dissolution pits are apparent in the upper right-hand quadrant. Regions highlighted with dashed circles are discussed in the text. Micrographs in C, continuing from the images shown in B, are obtained 320 min after introduction of 10^{-5} M Co^{2+}. Island growth is apparent in the pits. Micrographs i and ii show different locations on the same sample surface. Deflection-mode micrographs are 5.0 × 5.0 μm^2.

promoted pathways, might also be assisted by electrochemistry because a thermodynamically favorable process is the oxidation of aqueous Co^{2+} coupled to the reduction of manganese(III) (hydr)oxides.[24] If electrochemistry occurs, then Mn^{2+}(aq) dissolves to the aqueous phase while Co^{III} ions are incorporated in the growth of the new solid. In support of this possibility, Manceau et al. reported that aqueous Co^{2+} is oxidized by Mn^{III} in a hydrogen-rich birnessite.[23]

The chemical composition of the new islands contains at least some ions of oxidation states greater than 2+ (e.g., $Mn^{III/IV}$ or Co^{III}) because growth occurs only in the presence of dissolved O_2. Saturation calculations suggest that MnOOH, Mn_2O_3, MnO_2, Co_3O_4, and $Co(OH)_3$ could form under the measured [Mn^{2+}], [Co^{2+}], and pH conditions. Additional nanophase crystals not having known bulk-phase analogues (e.g., $Mn^{II}Co^{III}{}_2O_4$) might also be possible.[34]

Further evidence of the formation of a solid qualitatively different from the original manganese oxide film is the significant change in physical appearance. For example, whereas the height of the manganese oxide film is fixed at 2.4 nm, the islands constituting the new film have a continuous distribution (Figure 4). Moreover, the rounded versus rhombohedral growth in the presence versus the absence of Co^{2+}(aq) (Figure 5) is consistent both with an increased saturation ratio with respect to the solid[39] and with an increased lattice mismatch between the solid and the substrate. These differences demonstrate strong phase separation between the new solid and the initial manganese oxide film and imply that they have markedly different crystal structures.

An experiment that replaces the $MnCO_3$ substrate with a $MgCO_3$ substrate provides additional information on the nature of the new solid. Namely, under conditions of 10^{-5} M Co^{2+}(aq), 1 atm of dissolved O_2, and no aqueous Mn^{2+}, island formation is not observed on the $MgCO_3$ surface but is observed on the $MnCO_3$ surface. $MgCO_3$ and $MnCO_3$ have similar pH_{ZPC} values between 7.5 and 8.5 for low dissolved carbonate concentrations; therefore, differences in surface charge are unlikely to explain

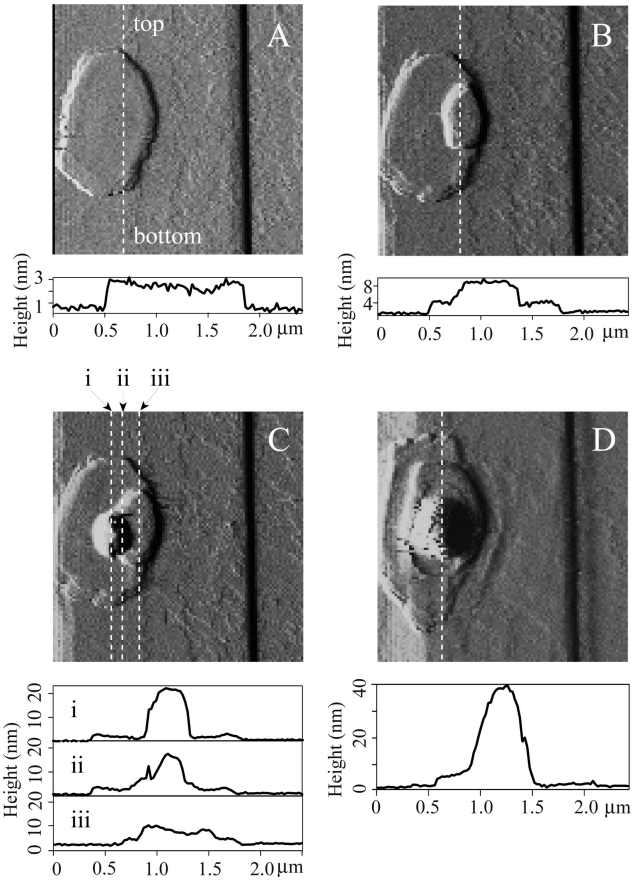

Figure 3. Cobalt ions promote film growth in the *z*-direction. Micrograph in A is obtained 1260 min after introduction of the cobalt-free aqueous solution. Growth in the vertical direction does not proceed higher than 2.4 nm. Micrograph B was obtained 90 min after introduction of 10^{-4} M Co^{2+}. The second layer of island nucleation allows further vertical growth of the oxide layer. Micrograph in C is obtained after 130 min. The third layer begins to grow. Micrograph in D is obtained after 540 min. Deflection-mode micrographs are 2.4 × 2.4 μm^2.

(39) Teng, H. H.; Dove, P. M.; De Yoreo, J. J. *Geochim. Cosmochim. Acta* **2000**, *64*, 2255−2266.

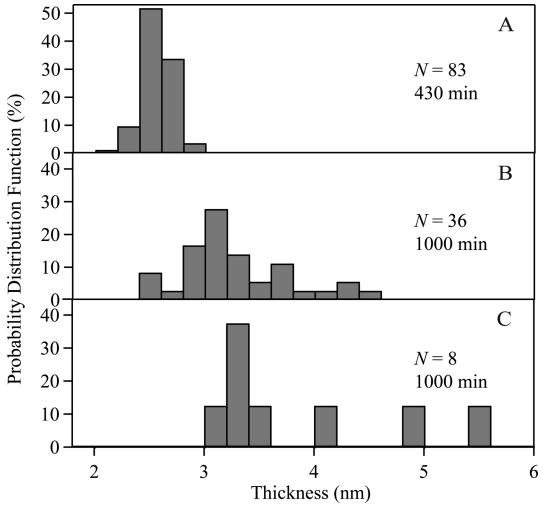

Figure 4. The probability distribution function of the island thickness depends on the preparation method (i.e., protocols 1−3). (A) No Co^{2+}(aq) is added. Rhombohedral manganese oxide islands form. The island height analysis is carried out 430 min after the experiment starts. (B) Manganese oxide islands are first grown. 10^{-5} M concentration of Co^{2+} is subsequently introduced, and new islands are grown. (C) 10^{-5} M Co^{2+} is introduced from the start. For B and C, the analysis of island heights is carried out 1000 min after the experiment starts. The number of islands included in the analysis is given in each panel.

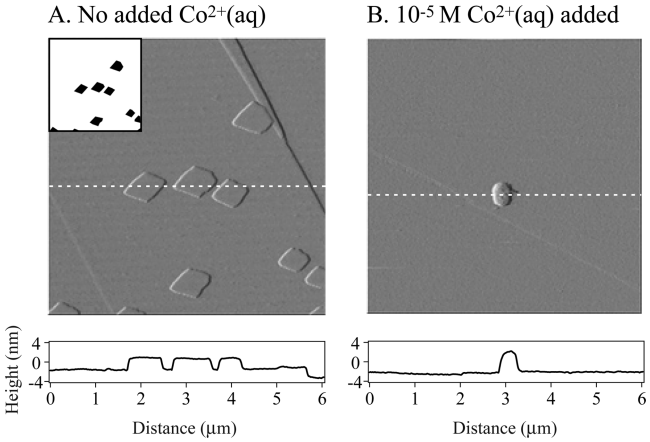

Figure 5. Island growth is altered by the presence of aqueous Co^{2+}. (A) In the absence of Co^{2+}(aq), the islands are rhombohedral in the lateral view and have flat tops in the cross-sectional view (94 min). (B) In the presence of 10^{-5} M Co^{2+}, the islands are irregular in the lateral view and have rounded tops (310 min). Locations of the height cross sections are indicated by the white dotted lines in the images. The AFM micrographs are shown in deflection mode ($6.0 \times 6.0\ \mu m^2$). (The inset of A is similar to the description given for Figure 2A.)

differences in island formation. Under the assumption that the $MgCO_3$ surface is equally as good as $MnCO_3$ toward heterogeneous nucleation, the absence of islands suggests that the Mn ion is a part of the stoichiometry of the new solid.

This suggestion is further backed by the macroscopic dissolution rate. The macroscopic dissolution rate, which is calculated by the difference in influent and effluent concentrations of $[Mn^{2+}]$,[36] is the net observable of three dissolution/growth processes, as follows:

$$R_{diss} = r_{diss,MnCO_3} + r_{diss,manganese\ oxide} + r_{new\ film} \qquad (1)$$

where $r_{diss,MnCO_3}$, $r_{diss,manganese\ oxide}$, and $r_{new\ film}$ are the respective dissolution rates (mol m^{-2} s^{-1}) of the $MnCO_3$ substrate, the manganese oxide film, and the new film. In the absence of cobalt, the macroscopic dissolution rate is $(3 \pm 1) \times 10^{-8}$ mol m^{-2} s^{-1} (ca. 0.01 monolayer s^{-1}). In the presence of cobalt, the average macroscopic dissolution rate decreases by no more than 50% for $[Co^{2+}](aq)$ ranging from 10^{-6} to 10^{-3} M. If Mn ions were not part of the new film, then the macroscopic dissolution rate should increase. Observation of the opposite trend provides further evidence that Mn ions are part of the new film.

The growth of the new film in the presence of cobalt differs in six key respects from the growth of the manganese oxide film in the absence of cobalt.

The first observation is that cobalt ions increase the height and the dispersion of the heights of the islands. In the absence of cobalt ions (i.e., protocol 1), the film height is 2.36 ± 0.14 nm (Figure 4A) and does not change with time. The statistical analysis of film heights is based upon measurements of 83 islands from 9 different samples. When cobalt ions are introduced, changes occur in the heights of the islands. Namely, when the manganese oxide film is formed and 10^{-5} M Co^{2+} is subsequently added (i.e., protocol 2), the islands thicken to approximately 3 nm and their dispersion increases (Figure 4B, height distribution of 3.1 ± 0.5 nm, $n = 36$). When 10^{-5} M Co^{2+} is added from the start of the experiment (i.e., protocol 3, Figure 4C), the dispersion of island heights increases compared to that of protocols 1 and 2. Moreover, for both protocols 2 and 3, the heights of the islands increase with time, and parts B and C of Figure 4 reflect a snapshot at 1000 min.

The second observation is that cobalt ions retard the nucleation and the growth of the new islands. In protocol 1, manganese oxide film growth is observable 100−300 min after the introduction of the aqueous solution (viz., patchy islands in Figure 5A). (Islands may be present but not observable earlier in the film growth: the limit in the lateral resolution of the atomic force microscope is that one pixel is 23 nm for the typically employed scan size of $12 \times 12\ \mu m^2$.) In contrast, in protocol 3, although film growth is also observed after 100−300 min, the islands have a much lower number density (Figure 5B). Moreover, the film growth rates based on volume changes with time (m^3 s^{-1}) are approximately 40 times slower in the presence of cobalt than in its absence.

The third observation is that cobalt ions alter island shapes. The island tops round in the *z*-direction, and the islands do not form rhombohedral shapes in the *x*-*y* plane (Figure 5B). Jun et al. report that island rounding occurs for high saturation ratios.[34] In protocol 1, the rounded islands return to a rhombohedral euhedral shape with further time. In protocols 2 and 3, however, the restoration of a euhedral shape is not observed. We hypothesize that a large lattice mismatch between the new solid and the $MnCO_3$ substrate causes an accumulation of strain that inhibits the restoration of a euhedral shape.

The fourth observation is that cobalt ions allow the nucleation and the growth of new islands in the dissolution pits present on the $MnCO_3$ surface (Figure 2). Islands do not form in the dissolution pits in the absence of cobalt (Figure 2B). After 10^{-5} M Co^{2+} is introduced, however, islands form in pits (Figure 2C). These islands appear to have random orientation with respect to the pit walls, and their formation occurs preferentially at obtuse steps of the dissolution pits. Concurrently, the manganese oxide film itself dissolves when Co^{2+}(aq) is introduced (dotted circles).

The fifth observation is that cobalt ions change the island growth mode. Namely, extended growth occurs in the *z*-direction for protocol 2, whereas the film height is limited to 2.7 nm in protocol 1. For example, the cross section in Figure 3A shows the height of the manganese oxide island in the absence of cobalt.

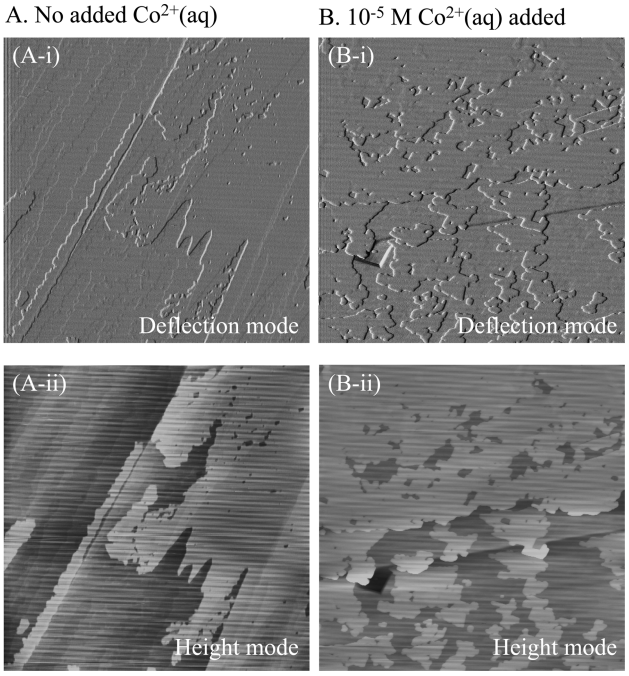

Figure 6. Islands grow over substrate steps in the presence of cobalt. Micrographs in A are obtained 413 min after introduction of the cobalt-free aqueous solution. Islands do not grow over steps. Micrographs in B are obtained 924 min after introduction of 10^{-5} M Co^{2+}. Islands cross over a step. Micrographs A and B are 13.6×13.6 and 7.7×7.7 μm^2, respectively. (i) Deflection-mode and (ii) height-mode micrographs are shown. (Panel A-i originally appeared as Figure 5C in ref 34. Copyright 2005 American Chemical Society.)

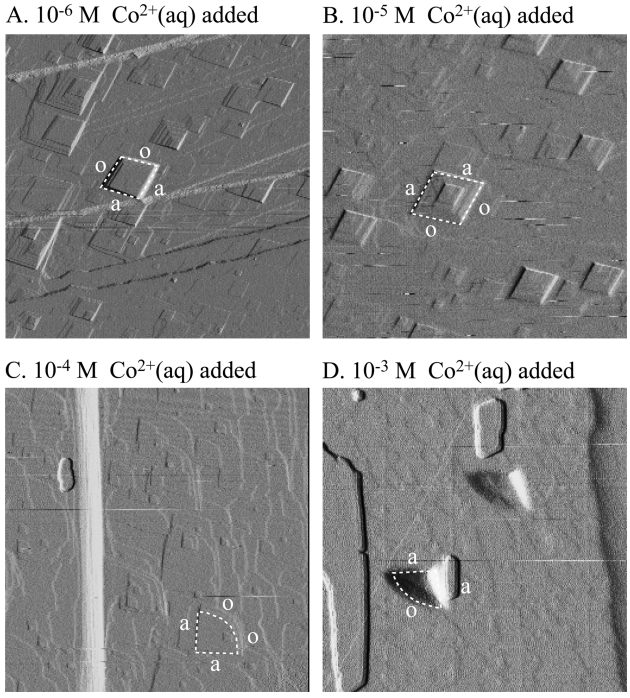

Figure 7. Cobalt ions affect the shape of the $MnCO_3$ dissolution pits. Micrograph in A is obtained 1130 min after introduction of 10^{-6} M Co^{2+}. Rhombohedral dissolution pits are apparent. Micrograph in B is obtained 1200 min after introduction of 10^{-5} M Co^{2+}. Micrograph in C is obtained 1540 min after introduction of 10^{-4} M Co^{2+}. The obtuse side of the dissolution pit is rounded. Micrograph in D is obtained 1400 min after introduction of 10^{-3} M Co^{2+}. Deflection-mode micrographs are 6.0×6.0 μm^2.

After cobalt is added into the systems, another island forms on the preexisting island to form a stratum structure (Figure 3B). Later, a third stratum also grows (Figure 3C), and even later, the island thickness reaches 40 nm (Figure 3D), compared to a maximum thickness of 2.7 nm in the absence of cobalt. These observations illustrate the broad thickness distribution apparent in parts B and C of Figure 4 in comparison to Figure 4A. Growth of strata, which is identifiable as Volmer−Weber growth,[40,41] occurs when the sum of the interfacial energies of the film against water ($\sigma_{f/w}$) and the substrate against the film ($\sigma_{s/f}$) exceeds the interfacial energy of the substrate against water ($\sigma_{s/w}$).[40]

The final observation is that cobalt ions allow island growth to cross over substrate steps (part A versus part B of Figure 6). The manganese oxide film does not propagate over steps in the absence of cobalt. Cobalt ions, therefore, relieve the two-dimensional restriction on layer formation and allow three-dimensional growth. We infer either (1) that cobalt ions decrease the energy barrier for diffusion of the growth monomer (i.e., the effects are large enough to overcome the Ehrlich−Schwoebel barrier at the steps[36,42]) or (2) that cobalt as a foreign ion distorts the lattice constant of the unit cell of the new film sufficiently to provide freedom to grow over the steps. The latter point is consistent with the loss of the euhedral island shape, as mentioned earlier in reference to Figure 5B.

In addition to effects on film growth, the presence of cobalt also affects the dissolution pit shape (Figure 7). Lower concentrations, including 10^{-6} and 10^{-5} M Co^{2+}, do not distort the pit shape. The pit shape is distorted, however, for 10^{-4} and 10^{-3} M Co^{2+}. Namely, there is rounding on the obtuse edges of the pit. Ionic radii, which are 0.75 Å for Co^{2+} ions[43] and 0.80 Å for Mn^{2+} ions,[44] could indicate preferential incorporation at obtuse steps: because the cobalt ion is nearly as large as the manganese ion, there may be steric hindrance for the incorporation of the cobalt ion at the acute step compared to that of the obtuse step of the $MnCO_3$ pit. The subsequent alteration of the pit shape can be explained by the terrace−ledge−kink (TLK) model,[45,46] as explained by Lea et al.[47] for the rounding of the dissolution pits of calcite in the presence of excess CO_3^{2-}(aq). For comparison, Reeder and Paquette[43,48] studied the incorporation of ions in specific directions on the calcite surface. Co^{2+} and Cd^{2+} ions were enriched along the acute step, possibly because of their smaller ionic radii. In contrast, Zn^{2+} and Ba^{2+} were enriched along the obtuse step. Freij et al.[49,50] reported that Co^{2+} and Zn^{2+} ions were incorporated at the acute and obtuse steps, respectively, in the $CaCO_3$ dissolution pits and that these ions distorted the rhombohedral pits into triangular ones.

4. Conclusions

The major mechanistic insights of the current study are depicted in Figure 8. At circumneutral pH and under oxygen-saturated

(40) Pimpinelli, A.; Villain, J. *Physics of Crystal Growth*; Cambridge University Press: Cambridge, U.K., 1998.
(41) Teichert, C. *Phys. Rep.* **2002**, *365*, 335−432.
(42) Schwoebel, R. L.; Shipsey, E. J. *J. Appl. Phys.* **1966**, *37*, 3682−3686.
(43) Reeder, R. J. *Geochim. Cosmochim. Acta* **1996**, *60*, 1543−1552.
(44) Zachara, J. M.; Cowan, C. E.; Resch, C. T. *Geochim. Cosmochim. Acta* **1991**, *55*, 1549−1562.
(45) Liang, Y.; Baer, D. R. *Surf. Sci.* **1997**, *373*, 275−287.
(46) Liang, Y.; Baer, D. R.; McCoy, J. M.; LaFemina, J. P. *J. Vac. Sci. Technol., A* **1996**, *14*, 1368−1375.
(47) Lea, A. S.; Amonette, J. E.; Baer, D. R.; Liang, Y.; Colton, N. G. *Geochim. Cosmochim. Acta* **2001**, *65*, 369−379.
(48) Paquette, J.; Reeder, R. J. *Geochim. Cosmochim. Acta* **1995**, *59*, 735−749.
(49) Freij, S. J.; Godelitsas, A.; Putnis, A. *J. Cryst. Growth* **2005**, *273*, 535−545.
(50) Freij, S. J.; Putnis, A.; Astilleros, J. M. *J. Cryst. Growth* **2004**, *267*, 288−300.

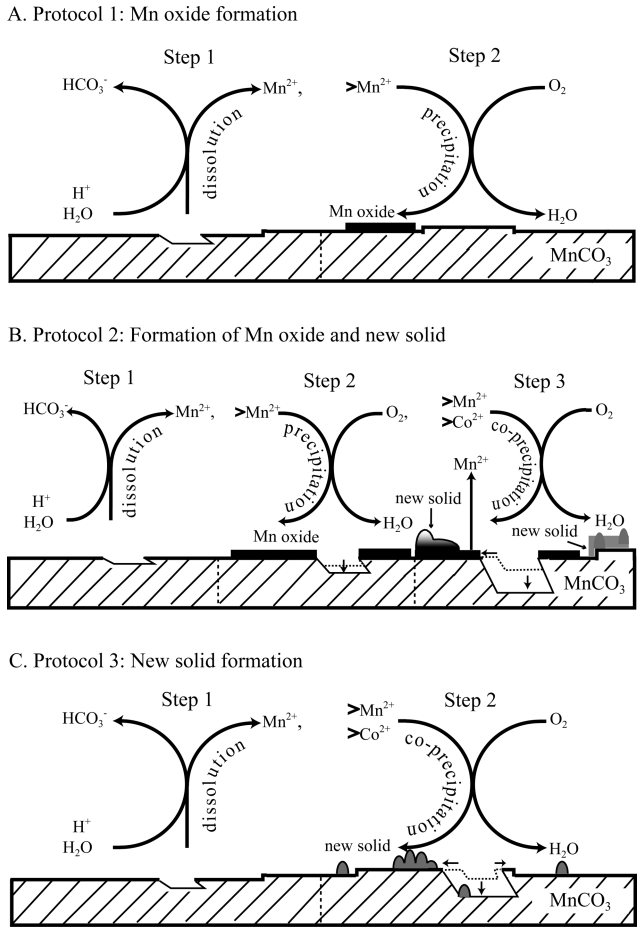

Figure 8. Proposed mechanisms of film formation in the absence and in the presence of aqueous cobalt. A $MnCO_3$ substrate under circumneutral pH and oxic conditions is assumed. $>Mn^{2+}$ and $>Co^{2+}$ denote surface-adsorbed species. Protocols 1−3 are described in section 2.3 of the text.

conditions, aqueous Mn^{2+} is released in the dissolution of $MnCO_3$ but adsorbs to the $MnCO_3$ surface as $>Mn^{2+}$. The surface catalyzes the oxidation of $>Mn^{2+}$ by O_2(aq). In the absence of other metal ions (Figure 8A), rhombohedral manganese oxide islands nucleate by heterogeneous oxidation on the $MnCO_3$ substrate, subsequently grow, and finally entirely cover the surface as a film. When cobalt ions are added after initial growth of the manganese oxide film, that film reverses its growth and is replaced by a new solid phase that nucleates and grows (Figure 8B). When cobalt ions are added at the beginning of the experiment, growth of the new solid proceeds immediately (Figure 8C).

The experimental results can be categorized into growth rules (i) in the absence of and (ii) in the presence of aqueous cobalt ions. In the absence of cobalt, islands grow as flat two-dimensional rhombohedra of 2.4 ± 0.3 nm height. The growth is capped in the *z*-direction and does not proceed over steps. Simultaneous with the film growth, rhombohedral dissolution pits are apparent.

The growth rules change considerably in the presence of cobalt ions. Namely, the islands grow indefinitely in the *z*-direction as strata structures of polydisperse thickness and rounded tops. The islands readily grow over steps. Cobalt ions, therefore, relieve the two-dimensional restriction on layer formation and allow three-dimensional growth. The shape of the pits that accompanies $MnCO_3$ dissolution is also distorted. Cobalt ions partition preferentially to the obtuse edge, which leads to a rounding of those edges of the pit.

The experimental results provide several constraints on the chemical composition of the new islands. They contain at least some ions of oxidation states greater than 2+ (e.g., $Mn^{III/IV}$ or Co^{III}) because growth occurs only in the presence of dissolved O_2. The rapid dissolution of the original manganese oxide film is suggestive of an electrochemical dissolution pathway in which Mn^{2+}(aq) dissolves to the aqueous phase while Co^{III} ions are incorporated in the growth of the new solid. The absence of film growth on $MgCO_3$ further suggests that the Mn ion is part of the new solid, which is further supported by the decrease of up to 50% in the macroscopic release rate of Mn^{2+}(aq) upon the addition of Co^{2+}(aq). The evidence as a whole thus suggests that the chemical composition of these new islands includes both Co and Mn.

The observations reported herein of the dynamic interactions of cobalt ions with manganese oxide films are important in the development of mechanistic, quantitative models of the effects of heavy metals on dissolution and precipitation of oxide films and, ultimately, of the adsorption/desorption and incorporation/release of the heavy metals in aquatic environments.

Acknowledgment. We are grateful for support received from the Petroleum Research Fund and the Chemical Sciences, Geosciences, and Biosciences Division of the Office of Basic Energy Sciences in the U.S. Department of Energy. Minerals were obtained from the collections of the Harvard University Mineralogical Museum. We thank Cynthia M. Friend, Carl Francis, and Joanne Aizenberg for valuable discussion.

Supporting Information Available: Time series images of Figures 1−3 and 5−7 (please note the scale difference between the movies and figures; the scales are indicated in the movies). This material is available free of charge via the Internet at http://pubs.acs.org.

LA0509450